



Probabilistic hazard analyses for a small island: methods for quantifying tephra fall hazard and appraising possible impacts on Ascension Island

Sara Osman¹ · Julia Crummy² · Mark Thomas¹ · Stephen Carver³

Received: 20 November 2023 / Accepted: 8 September 2024 / Published online: 20 September 2024
© The Author(s) 2024

Abstract

Proximal to the source, tephra fall can cause severe disruption, and populations of small volcanically active islands can be particularly susceptible. Volcanic hazard assessments draw on data from past events generated from historical observations and the geological record. However, on small volcanic islands, many eruptive deposits are under-represented or missing due to the bulk of tephra being deposited offshore and high erosion rates from weather and landslides. Ascension Island is such an island located in the South Atlantic, with geological evidence of mafic and felsic explosive volcanism. Limited tephra preservation makes it difficult to correlate explosive eruption deposits and constrains the frequency or magnitude of past eruptions. We therefore combined knowledge from the geological record together with eruptions from the analogous São Miguel island, Azores, to probabilistically model a range of possible future explosive eruption scenarios. We simulated felsic events from a single vent in the east of the island, and, as mafic volcanism has largely occurred from monogenetic vents, we accounted for uncertainty in future vent location by using a grid of equally probable source locations within the areas of most recent eruptive activity. We investigated the hazards and some potential impacts of short-lived explosive events where tephra fall deposits could cause significant damage and our results provide probabilities of tephra fall loads from modelled events exceeding threshold values for potential damage. For basaltic events with 6–10 km plume heights, we found a 50% probability that tephra fallout across the west side of the island would impact roads and the airport during a single explosive event, and if roofs cannot be cleared, three modelled explosive phases produced tephra loads that may be sufficient to cause roof collapse ($\geq 100 \text{ kg m}^{-2}$). For trachytic events, our results show a 50% probability of loads of 2–12 kg m^{-2} for a plume height of 6 km increasing to 898–3167 kg m^{-2} for a plume height of 19 km. Our results can assist in raising awareness of the potential impacts of tephra fall from short-lived explosive events on small islands.

Keywords Volcanic hazards · Ascension Island · Tephra fall impacts · Built environment · Roof collapse

Introduction

Tephra is produced in all explosive volcanic eruptions, with a range of observed impacts depending on the size and duration of the eruption and proximity to the source. For communities in volcanically active areas, airborne or remobilised tephra can lead to health issues (IVHHN 2021; Stewart et al. 2022; Eychenne et al. 2022) while deposits can cause significant disruption depending on their thickness and the loading placed on structures (Table 1). Accumulations of $< 1 \text{ mm}$ ($\sim 1 \text{ kg m}^{-2}$ depending on deposit density) can affect roads and airports, with markings covered and increased skid risk (Blake et al. 2017). Tephra loads of 1–10 kg m^{-2} (thickness $\sim 1\text{--}10 \text{ mm}$) can damage power, water and communications networks and severely disrupt

Editorial responsibility: A. Tadini

✉ Sara Osman
eesjo@leeds.ac.uk

¹ School of Earth and Environment, University of Leeds, Woodhouse, Leeds LS2 9JT, UK

² British Geological Survey, The Lyell Centre, Research Avenue South, Edinburgh EH14 4AP, UK

³ School of Geography, University of Leeds, Woodhouse, Leeds LS2 9JT, UK

Table 1 Summary of likely impacts at different tephra fall loads (amended from Jenkins et al. 2014)

Tephra load (kg m ⁻²)	Likely impact
1	Increased skid risk and markings covered at airports and on roads
10	Damage to power, water and communications networks Severe impact to roads and closure of airports Impact on crops, depending on the stage in the growth cycle
100	Collapse of weakest roofs
150	Collapse of long-span roofs
300	Collapse of good quality metal roofs
400	Collapse of good quality tile roofs
700	Collapse of good quality concrete roofs

road and rail travel (Jenkins et al. 2015; Blake et al. 2017; Hayes et al. 2022). At these loads, crops can suffer discoloration or loss of leaves and abrasion or rotting of fruit, but the severity depends on the stage of the crop development cycle (Jenkins et al. 2015; Wilson et al. 2017; Ligot et al. 2022). Tephra loads ~ 100 kg m⁻² have been observed to cause extensive infrastructure damage and result in the collapse of the weakest roofs, while loads above ~ 150 kg m⁻² have the potential to cause significant roof damage or collapse regardless of condition (Jenkins et al. 2014; Wilson et al. 2014; Hayes et al. 2022). Post-depositional rainfall may increase deposit density (and hence loading) by up to 45%, depending on tephra grain size and rainfall intensity (Hayes et al. 2019; Williams et al. 2021).

Populations of small volcanically active islands can be especially susceptible to the impacts of tephra fall because of their proximity to the vent. It is therefore crucial to understand this potential hazard to aid in planning for possible future explosive events. However, there are large uncertainties associated with the limited geological data, as small ocean islands often have significant gaps in our knowledge of their eruptive history. This is due to a substantial proportion of tephra being deposited offshore, high erosion rates from rainfall and wind and the susceptibility of volcanic islands to landslides. To address these knowledge gaps, we can use data from well-studied analogue volcanoes to model possible future events (e.g. Hone et al. 2007; Cashman and Biggs 2014; Tierz et al. 2019; Burgos et al. 2023).

To gain a better understanding of tephra fall hazard and impact on a remote island, we have carried out an exploratory probabilistic tephra fall hazard analysis for Ascension Island in the South Atlantic (referred to as Ascension hereafter) for a range of discrete, short-lived explosive events from selected vent locations across the island. Ascension is a strategically important UK Overseas Territory, located ~ 90 km

west of the mid-Atlantic ridge in the South Atlantic Ocean, with an area of ~ 98 km² and ~ 780 residents (Fig. 1). Key infrastructure includes the airport, Royal Air Force (Travelers Hill) and US Air Force (USAF) bases, the South Atlantic Relay communications station, a power plant and the small settlements of Georgetown and Two Boats (Fig. 1). Ascension has been volcanically active for ~ 6 Ma, and recent research has given insights into its magmatic history, with deposits providing evidence for past effusive and explosive eruptions of both mafic and felsic composition (e.g. Chamberlain et al. 2016, 2019, 2020; Winstanley 2020; Preece et al. 2021; Davies et al. 2021). The most recent known effusive eruptive activity has been dated to 510 ± 180 years ago (Preece et al. 2018); however, poor tephra preservation (with deposits missing from the record and units being untraceable across the island) means that past explosive eruptions are not well constrained (Preece et al. 2021). We have therefore used eruption source parameters from analogue eruptions together with published geological data to model a range of possible future explosive events and discuss potential impacts on infrastructure.

Tephra fall is, of course, just one of the potential volcanic hazards that are considered in comprehensive hazard and impact assessments, which often use event trees to quantify the likelihood of each hazard (including lava flows, pyroclastic density currents and lahars, as well as tephra fall) (e.g. Newhall and Hoblitt 2002; Marzocchi et al. 2012; Tadini et al. 2021; Alatorre-Ibargüengoitia et al. 2021). Such full assessments are beyond the scope of this work, in which we consider only a subset of events, where the additional loading on roofs due to tephra fall deposits may lead to collapse. Because of the knowledge gaps in Ascension's eruptive history (Preece et al. 2021), it is difficult to assess the frequency of these large explosive events. Our results therefore provide conditional probabilities of tephra fall loads exceeding threshold values; i.e. we assume that an explosive event has occurred. If future research provides more detailed data on the eruptive history of Ascension, our results could be combined with the probabilities of such events occurring to produce unconditional probabilities (Connor et al. 2015).

Geological background

The volcanic edifice of Ascension Island is built on oceanic crust from ~ 7 Ma, with borehole evidence suggesting subaerial eruptions began ~ 2.5 Ma and the oldest surface deposits dated to ~ 1 Ma (Minshull et al. 2010; Jicha et al. 2013). Eruptive products cover the full compositional range from basalt to rhyolite, with alkaline felsic magmas produced by fractional crystallisation in a closed system (Weaver et al. 1996; Kar et al. 1998; Jicha et al. 2013; Chamberlain et al. 2016). This pattern is also seen at other ocean islands, e.g.

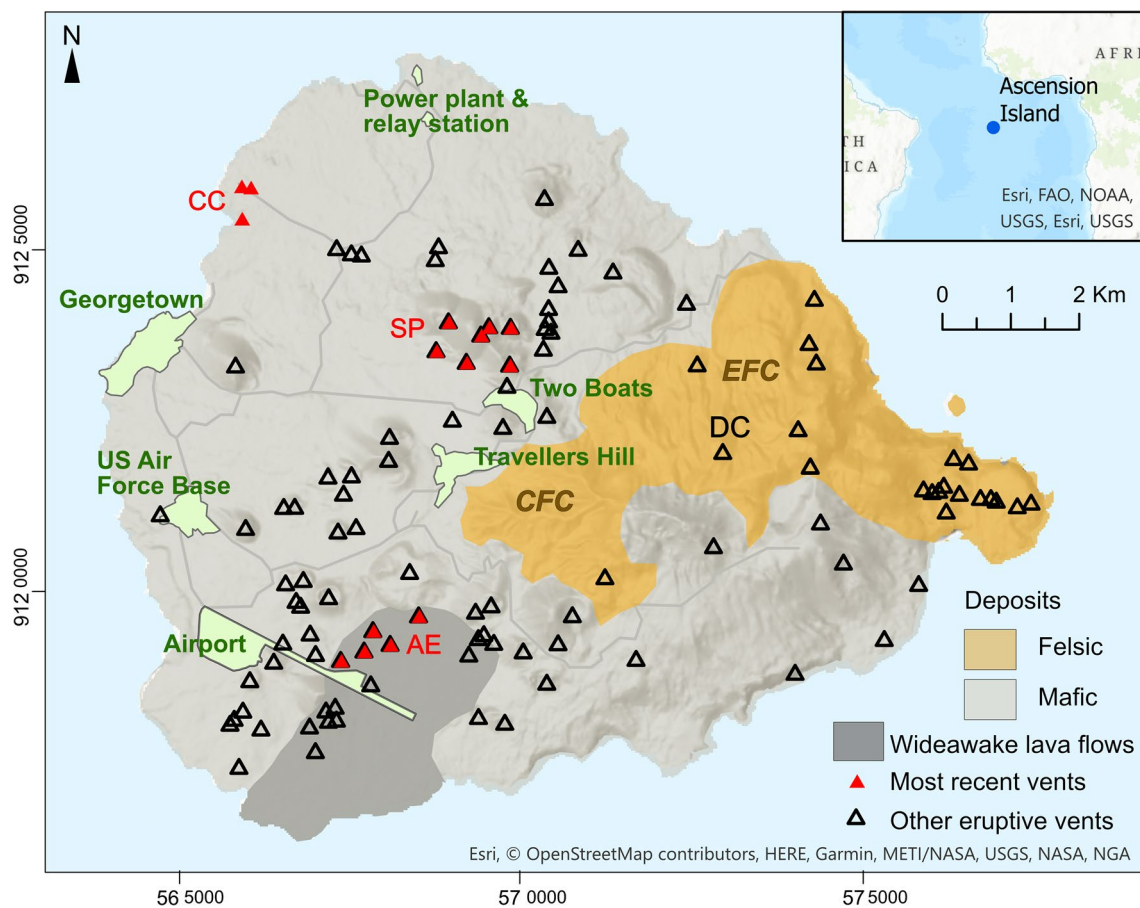


Fig. 1 Map of Ascension Island showing main settlements and infrastructure, eruptive vents and approximate areas of felsic and mafic volcanism. CFC, Central Felsic Complex; EFC, Eastern Felsic Complex. Eruptive vent: DC, Devil's Cauldron vent. Most recent vents: CC, Comfortless Cove; SP, Sister's Peak; AE, Airport East. Mafic

and felsic deposits amended from Chamberlain et al. (2020), the extent of Wideawake lava flows from Nielson and Sibbett (1996), vent locations from Vye-Brown et al. (2019). Coordinate reference system: WGS84/UTM 28S

São Miguel, Azores (Widom et al. 1992; Guest et al. 1999; Jeffery et al. 2016). Alkali basalt and hawaiite scoria cones and flows occur widely across the island, while trachyte and rhyolite domes, flows and pyroclastics are concentrated in the centre and east (Nielson and Sibbett 1996; Weaver et al. 1996; Hobson 2001; Jicha et al. 2013). This spatial separation of mafic and felsic volcanism suggests a crustal control on composition and has been interpreted to result from low magma flux (Chamberlain et al. 2019). Pyroclastic deposits contain peralkaline xenoliths (Harris 1983).

Subaerial eruptive activity on Ascension has followed a cyclic pattern with periods of predominantly felsic volcanism (~1 Ma–500 ka from the Central Felsic Complex; ~100–50 ka from the Eastern Felsic Complex (Fig. 1)) alternating with mafic eruptive periods (~500–100 ka; < ~50 ka). At least 80 explosive felsic eruptions have occurred over the past 1 Ma, including 11 pumice-forming eruptions between ~100 and 60 ka (Preece et al. 2021). Deposits up to 40 m thick provide

evidence of magmatic and phreatomagmatic eruptions spanning a range of sizes (Daly 1922; Atkins et al. 1964; Nielson and Sibbett 1996; Preece et al. 2018, 2021; Davies et al. 2021). Outcrops are limited and stratigraphic correlation is only possible over short distances, meaning it is often not possible to identify vent locations or estimate erupted volumes, particularly for older eruptions (Preece et al. 2021). However, analyses of deposits from individual eruptions in the Eastern Felsic Complex have greatly increased the understanding of eruptive processes on the island. These include a fall deposit zoned from trachytic pumice at the base to trachy-basaltic andesite scoria at the top provides evidence of closed system fractional crystallisation (Chamberlain et al. 2016) and deposits from one small volume (0.01–0.3 km³) eruption showing evidence of lava flows, Strombolian explosions and transient Plinian activity (Davies et al. 2021). In addition, a mingled fall deposit found at several outcrops in the centre of the island suggests mafic melt mixing with rhyolitic magma

in a shallow magma chamber around 24 h before eruption (Chamberlain et al. 2020).

Mafic eruptions occur from monogenetic vents (shown in Fig. 1). $^{40}\text{Ar}/^{39}\text{Ar}$ dating of the youngest lava flows gave ages of 510 ± 180 years and indicated the most recent eruptive areas are around Comfortless Cove and Sister's Peak (Preece et al. 2018). Recent basaltic activity also produced the Wideawake lava flows to the east of the airport (Vye-Brown et al. 2019; Vye-Brown pers. comm).

Methods

Our simulations considered discrete explosive events (our model scenarios) with eruptive plumes ranging from 6 to 27 km above sea level (a.s.l.) and durations of 1–12 h. While the reasoning for the location of the events is discussed further in the 'Selection of model scenarios' section, this study assumes that an event will occur at the chosen locations without explicitly assessing the likelihood of that event. For each model scenario, we assessed the probability of tephra fall loads reaching the reported failure thresholds for different roof types.

Despite the geological data on Ascension in the published literature, there are large uncertainties around the eruption source parameters, plume heights, erupted volumes and grain size distributions. We therefore make assumptions based on previous work (Vye-Brown et al. 2019) and the tephra modelling literature (detailed in Tables 2 and 3) and rely on analogues to derive the input parameters for our model scenarios (detailed in the 'Selection of analogues' section).

Selection of analogues

Based on the geological setting, geochemistry of eruptive products and deposit characteristics, we use the oceanic island of São Miguel in the Azores as an analogue for Ascension. São Miguel exhibits a wide compositional range of erupted products, formed by fractional crystallisation in a low magma flux environment with spatial separation of peralkaline felsic and mafic eruptions (Widom et al. 1992; Guest et al. 1999; Jeffery et al. 2016). The eruptive history for the past 5 ka is well constrained, with trachytic eruptions from Sete Cidades, Fogo (Água de Pau) and Furnas volcanoes and basaltic activity in the Picos and Congro Fissural Volcanic Systems (Guest et al. 1999). The well-studied peralkaline, trachytic deposits of the Fogo A (4.6 ka, plume height 21–30 km) and Fogo 1563 (plume height ~ 19 km) eruptions (Carey and Sigurdsson 1989; Guest et al. 1999; Pensa et al. 2015) enable estimates of eruption source parameters to be made for future large, felsic eruptions. These provide good analogues for the thick pyroclastic

deposits of alkaline trachyte on Ascension (Chamberlain et al. 2019; Preece et al. 2021). Thirty-six basaltic eruptions have occurred over the past 5 ka in the Picos Fissural Volcanic System (Gaspar et al. 2015). The Serra Gorda eruption (3–5 ka), estimated at VEI 3, produced the largest scoria cone in this system with deposits 50 cm thick at distances up to 4 km from the source (Booth et al. 1978; Newhall and Self 1982; Ferreira et al. 2015). Although there are many examples of smaller eruptions of this type, including on Ascension (Winstanley 2020), we consider this eruption a good analogue for the scale of monogenetic volcanism on Ascension that might produce tephra fall deposits sufficient to cause roof collapse (hence of interest to this study), without commenting on the likelihood of an event of this size.

Selection of model scenarios

Our simulations build on expert elicitation and initial modelling carried out by the British Geological Survey to quantify the tephra fall hazard on Ascension Island (Vye-Brown et al. 2019). That work produced some preliminary probabilistic tephra fall footprints for three felsic scenarios with plume heights of 6, 17 and 27 km a.s.l. from Devil's Cauldron using 30 days of wind data. Tephra fall simulations revealed that even a small eruption on the island would likely disperse tephra across the whole island (Vye-Brown et al. 2019). We have used this as a baseline for detailed tephra fall hazard analysis by considering a range of scenarios for felsic and mafic explosive events (detailed in the 'Felsic events' and 'Mafic events' sections respectively), using a 10-year reanalysis wind dataset ('Wind data' section). This study specifically aims to quantify tephra fall hazard from a range of possible explosive events where deposit loads may lead to significant roof damage. Both the felsic and mafic explosive events were modelled using eruption source parameters from our selected analogue eruptions in São Miguel.

Felsic events

We simulated explosive, trachytic events from the Devil's Cauldron vent (Fig. 1) in the Eastern Felsic Complex, with plume heights of 6–27 km a.s.l. This was the assumed vent for an eruption ~ 65 ka; however, this is likely a worst case, as felsic volcanism has moved eastwards over time (Preece et al. 2021). To investigate potential impacts from specifically large events, we ran simulations with 19 and 27 km plume heights, based on the Fogo 1563 and Fogo A eruptions on São Miguel (Walker and Croasdale 1970; Carey and Sigurdsson 1989; Gaspar et al. 2015; Pensa et al. 2015). We also simulated smaller volume events (Davies et al. 2021) with 6, 12 and 15 km plume heights.

Table 2 Input parameters used for felsic simulations

Plume height (km a.s.l.)	Mass erupted (kg)	Duration (h)	Rationale
27	10^{11} – 5×10^{12}	3–12	Selected to best match Fogo 1563 and Fogo A eruptions (Walker and Croasdale 1970; Carey and Sigurdsson 1989; Gaspar et al. 2015; Pensa et al. 2015)
19	10^{10} – 10^{12}	2–6	
15	10^{10} – 5×10^{11}	1–4	Selected to model smaller volume eruptions (e.g. Davies et al. 2021)
12	10^9 – 10^{11}	1–3	
6	10^7 – 10^{10}	1–3	
Parameters used for all felsic simulations			
Parameter	Value	Rationale	
Total grain size distribution ϕ range (Md ϕ)	–5 to 6 (0.5)	Based on published grain size distributions for Fogo 1563 and Fogo A eruptions (Walker and Croasdale 1970)	
Standard deviation of grain size	2		
Aggregation	No		
Particle densities			Scollo (2008) found particle density has a negligible effect on modelled tephra loads, and so, we used typical values for trachytic tephra deposits on São Miguel (Kueppers et al. 2019)
ρ lithic (kg m^{-3})	2400		
ρ pumice (kg m^{-3})	800		
Model parameters			Selected so that tephra loads best matched observed Fogo A deposit (with tephra depths converted to loads using published deposit density of 500 kg m^{-3}) (Walker and Croasdale 1970). β distributions reflect the vertical distribution of mass in the plume. We tested:
Diffusion coefficient (m s^{-2})	5000		• $\alpha = 1, \beta = 1$ (mass evenly distributed)
Fall time threshold (s)	6000		• $\alpha = 2, \beta = 2$ (mass concentrated at the centre of the plume)
Plume model	1,1		• $\alpha = 3, \beta = 2$ (mass concentrated towards plume top)
β distribution (α, β)			• $\alpha = 2, \beta = 3$ (mass concentrated towards plume bottom)
Column integration steps	50		Produced stable load contours while optimising run time

Table 3 Input parameters used for mafic simulations

Parameter	Value	Rationale
Plume height (km a.s.l.)	6–10	Selected to simulate a relatively small eruption, but one that could lead to tephra deposits likely to cause roof collapse. 6 km was the minimum plume height where deposit loads reached roof collapse values beyond the vent area
Mass erupted (kg)	10^9 – 10^{10}	
Duration (h)	1–6	Based on maximum and median grain size data from the Serra Gorda eruption (Booth et al. 1978)
Total grain size distribution Φ range (Md Φ)	–5 to 5 (–1)	
Standard deviation of grain size	2	Scollo (2008) found particle density has a negligible effect on modelled tephra loads, and so, we used typical values (https://volcanoes.usgs.gov/volcanic_ash/density_hardness.html)
Aggregation	No	
Particle densities		Selected to best match observed Serra Gorda deposit (Booth et al. 1978) (with tephra depths converted to loads using an estimated deposit density of 1000 kg m^{-3}). β distributions reflect the vertical distribution of mass in the plume. We tested:
ρ lithic (kg m^{-3})	2900	
ρ pumice (kg m^{-3})	1000	<ul style="list-style-type: none"> • $\alpha = 1, \beta = 1$ (mass evenly distributed) • $\alpha = 2, \beta = 2$ (mass concentrated at the centre of the plume) • $\alpha = 3, \beta = 2$ (mass concentrated towards plume top) • $\alpha = 2, \beta = 3$ (mass concentrated towards plume bottom)
Model parameters		
Diffusion coefficient (m s^{-2})	4000	
Fall time threshold (s)	5000	
Plume model	2, 2	Produced stable load contours while optimising run time
β distribution (α, β)		
Column integration steps	50	

Mafic events

To investigate an explosive basaltic event with tephra fall deposits that may cause significant roof damage, we ran simulations based on the São Miguel Serra Gorda eruption (Booth et al. 1978). Our model scenarios used vent locations in each of the three recent eruptive areas, namely Comfortless Cove (CC), Sister's Peak (SP) and Airport East (AE), and modelled a single event with plume heights sampled in the range 6–10 km. We also explored the tephra fall footprint and potential impacts from multiple explosive pulses during an eruption, as observed during the 2021 eruptions at Soufrière St Vincent (Miller et al. 2022) and Cumbre Vieja, La Palma (Bonadonna et al. 2022; Martí et al. 2022), by simulating three pulses of activity, each with 6–10 km plume heights. It can be difficult to clear tephra deposits from roofs proximal to the source because of the possibility of ongoing volcanic activity and the risk of injuries due to falls from roofs or ladders (Wardman, et al. 2012; Magill et al. 2013). We therefore summed the loads from each pulse, simulating a worst-case scenario where roofs were not cleared and there was no erosion of the fall deposit between explosive phases. It is important to note that we are not simulating multiple separate eruptions or multiple vents in this scenario. We model pulses or phases of a single eruption where eruptive activity has stabilised to a dominant, main vent location. Multi-vent eruptions are also a possible scenario, and a similar approach to the one considered here can also be used to simulate these conditions through an appropriate sampling of the modelled tephra fall data for multiple vent locations.

Accounting for uncertainty in vent location

Many mafic eruptions on Ascension have occurred from monogenetic vents, but assessing the risk from monogenetic volcanic fields is difficult due to uncertainty with respect to the location of future vents (Valentine and Connor 2015). From Fig. 1, it is clear that eruptive activity has occurred over most of the island, but spatial density analysis has shown the highest density of monogenetic vents is found around Sister's Peak and across a wide area in the south, as well as in the far east of the island where eruptions of intermediate composition have occurred (Vye-Brown et al. 2019). However, gaps in the eruptive record make it difficult to undertake a full spatio-temporal hazard estimation (e.g. Kósik et al. 2020), and so, we chose to focus on areas of most recent activity as source locations for our model simulations. Selection of a single vent location for simulations can underestimate the area over which tephra loadings may exceed given thresholds compared to modelling a spread of possible vent locations. We therefore used a novel approach to model multiple possible vent locations within a specified area to consider a wider spread of tephra impacts, given the uncertainty of vent location. While we do consider multiple vent locations for a potential future eruption, as previously noted, phases or pulses of explosive activity for an individual eruption are considered to occur from a single stable vent location.

The lack of a clear temporal distribution or any unrest signals makes it difficult to define the potential location of any future eruption. In the absence of these data, we defined an area in which an assumed new vent could occur by creating a buffer around the most recent vents. For the

youngest vents in both the Sister’s Peak and Airport East areas, the average spacing between the vents has been estimated at ~400 m (Vye-Brown et al. 2019). We therefore imposed that the source of a future eruption would be within 400 m of these historical vents. Within this buffer area, we created a grid of vents with an equal probability of eruption and selected a grid spacing of 200 m, to ensure meaningful differences in model outputs, balanced against computational resource to run multiple simulations (Fig. 2). For Comfortless Cove, on the west of the island, the prevailing winds from the south-east would result in

most tephra being deposited over the sea with vent location having little impact on tephra loads on land; therefore, for this location, our scenarios were based on a single vent. This approach is taken in the absence of any other data on the likelihood of any new vent locations. Of course, the probability of a new vent forming elsewhere on the island is not zero. The results therefore should not be taken as a full hazard analysis as it will likely underestimate the hazard for other areas of the island. Rather, this approach demonstrates the methods that would be utilised if more data on possible future vent locations were available.

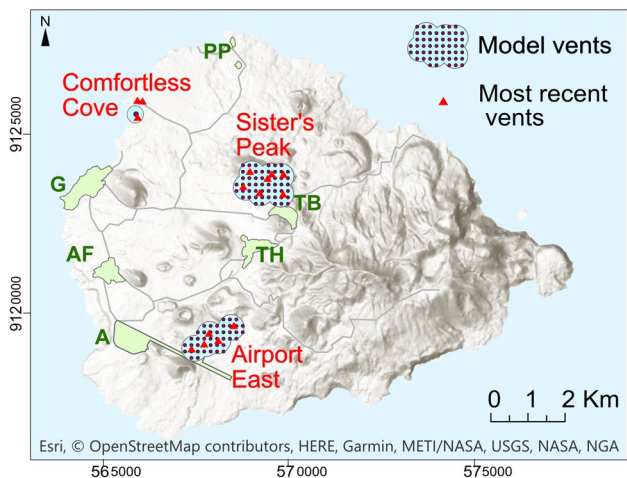
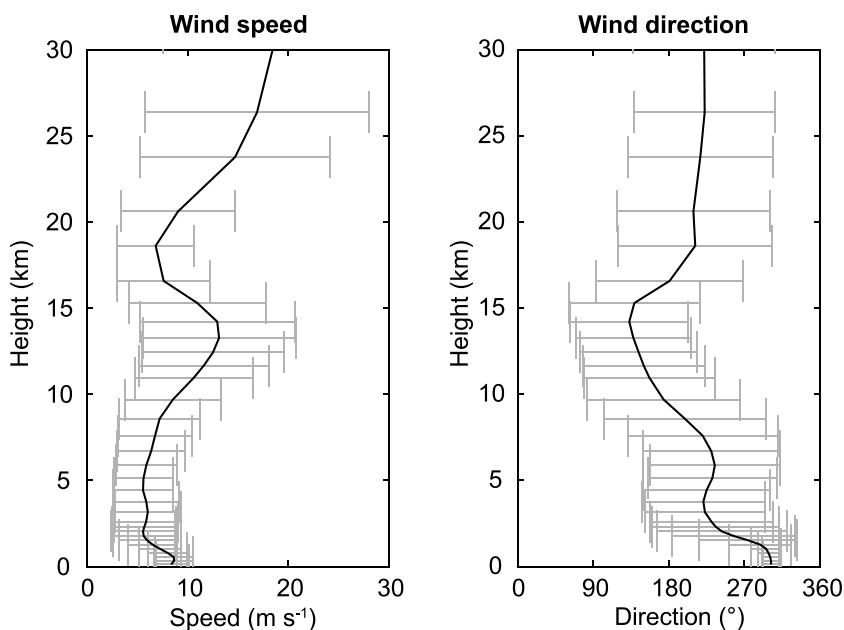


Fig. 2 Areas of most recent volcanism on Ascension and grid of model vents used for mafic eruptive scenarios. Key locations: A, airport; G, Georgetown; PP, power plant and South Atlantic Relay station; TB, Two Boats; TH, Travellers Hill; AF, US Air Force Base. Coordinate reference system: WGS84/UTM 28S

Wind data

Wind velocity influences the direction of the spread of the volcanic plume as well as the sedimentation of tephra, which controls the extent of the tephra footprint on the ground. We took account of variations in the wind field by stochastically sampling wind velocity from a 10-year ERA5 dataset for Ascension. The ERA5 reanalysis data covered the period 2010–2019 and comprised 6-hourly wind data at 37 pressure levels within the atmosphere with a horizontal resolution of ~30 km (Hersbach et al. 2018, 2020). To investigate seasonal variability, we analysed wind speed and direction by month using TephraProb (Biass et al. 2016). Wind roses for 3-monthly intervals at heights up to ~30 km above sea level (covering the heights of our simulated plumes) did not show significant seasonal trends (Fig. S1 in Supplementary material), and therefore, we sampled winds from the whole 10-year dataset for each of our simulations (14,608 wind profiles in total) (Fig. 3).

Fig. 3 Summary of wind conditions on Ascension Island (mean speed and mean direction that the wind is blowing towards) from the ERA5 2010–2019 reanalysis dataset (Hersbach et al. 2018) stochastically sampled for all simulations



Tephra modelling

We used Tephra2 with the TephraProb Matlab package for our probabilistic hazard modelling (Bonadonna et al. 2005; Connor and Connor 2006; Biass et al. 2016). Tephra2 takes inputs defining eruptive conditions (plume height, eruption duration, total mass erupted, grain size distribution, particle density) and solves the advection–diffusion equation in two dimensions to calculate tephra accumulation on the ground. The model uses a wind field that is assumed to be vertically stratified but horizontally constant, an assumption that is likely to be valid over the small area of Ascension. However, it does not account for small-scale atmospheric features such as eddies or temporal changes within the timescale of each wind profile (in our case 6 h). TephraProb enables multiple runs of Tephra2, with input parameters sampled within user-defined ranges, to be combined into a probabilistic output. Both Tephra2 and TephraProb have been widely used, and the outputs are now routinely accepted in scenario-based tephra fall hazard assessments of possible future events (e.g. Wild et al. 2019; Warwick et al. 2022; Aravena et al. 2023) and inversion modelling to recreate past events (e.g. Constantinescu et al. 2024; Crummy et al. 2019; Jenkins et al. 2020; Tennant et al. 2021). Tephra2 also assumes that the specified input parameters are representative of average conditions during peak eruptive activity (Connor and Connor 2006). Hence, events modelled here do not fully reflect the waxing and waning of an ongoing eruption with multiple explosive phases, as observed at the 2021 eruptions at Soufrière St Vincent (Cole et al. 2024) and Cumbre Vieja, La Palma (Martí et al. 2022), but rather treat each event as a discrete explosion.

We used analogue eruptions on São Miguel to calibrate the model and select best-fit values for model variables (including diffusion coefficient, fall time threshold and the plume model) which describe the release, transport and deposition of particles. Details of our model calibration are included in the Supplementary material, with the source parameters from the analogue eruptions shown in Table S1. The input parameters selected for our Ascension Island simulations are detailed in Tables 2 (felsic scenarios) and 3 (mafic scenarios).

For all our simulations, we accounted for uncertainty in meteorological conditions by randomly selecting a wind profile from the ERA5 2010–2019 dataset for each simulation. The tephra mass loading grid (the hazard grid) was defined to cover the entire island with a grid spacing of 500 m, which was found to be sufficient to resolve spatial variations in mass load.

Each felsic scenario from Devil’s Cauldron vent consisted of 1000 simulations where plume height was fixed and event duration was sampled uniformly within a range (Table 2). Values were constrained so that combinations of duration and mass eruption rate (calculated within TephraProb from plume height and wind data using Degruyter and Bonadonna (2012)) were only selected for the simulations when the resulting total erupted mass fell within the ranges defined based on our analogue eruptions (Biass et al. 2016).

For each mafic scenario, plume height was sampled within the range of 6–10 km, using a logarithmic distribution to account for small eruptions occurring more frequently than large ones, with combinations of plume height, duration and total mass erupted constrained as for the felsic simulations. For each scenario, we ran 1000 simulations for the single vent at Comfortless Cove (CC) and 1000 simulations from each potential vent within the Sister’s Peak (SP) and Airport East (AE) areas (53 vents for SP; 42 vents for AE) (Fig. 2 and Table S2).

For felsic simulations and mafic simulations from CC, with a fixed vent location (v), the probability of exceedance of tephra load above some threshold is estimated for each hazard grid location (defined by easting, E , and northing, N) as shown in Eq. 1.

$$P[l_{E,N} > T | \text{eruption from } v] \approx \frac{n}{N} \quad (1)$$

where T is the mass load threshold and $l_{E,N}$ is the estimated mass load at the location of the hazard estimate, specified by coordinates (E, N).

The number of simulations for which $l_{E,N} > T$ is n of a total of N simulations.

For our SP and AE scenarios, we used a grid of potential vent locations to investigate an eruption from a new vent within each area, A . Each vent location, i represents a small area, a_i , defined by the grid spacing within A . For grid spacing of Δx and Δy in the x (east) and y (north) directions respectively, i represents an eruption within the small area, $a_i = \Delta x \times \Delta y$. We assume the vent location grid spacing is sufficiently small that tephra loading at $l_{E,N}$ from an eruption at i is insignificantly different from results for a vent located anywhere within a_i . In this case, for simulations run from vent i , Eq. 1 is modified to Eq. 2:

$$P[l_{E,N} > T | \text{eruption within } a_i] \approx \frac{n_i}{N_i} \quad (2)$$

where n_i represents the number of simulations for which $l_{E,N} > T$, of a total of N_i simulations.

The total source area $A = M \Delta x \Delta y$, where M is the total number of grid points for vent locations within A ($M = 53$ and $M = 42$ for Sister’s Peak and Airport East areas respectively). As previously discussed, our scenarios assume that the probability of an eruption within $A = 1$ and is zero elsewhere. Hence, Eq. 3 shows the probability of exceedance of tephra load above some threshold for each hazard grid location for an eruption within A .

$$P[l_{E,N} > T | \text{eruption within } A] \approx \sum_{i=1}^M P[l_{E,N} > T | \text{eruption within } a_i] P[a_i | A] \tag{3}$$

where $P[a_i | A]$ is the probability of the vent being located within the small area a_i , given an eruption within A . We also assume that the probable vent location within A is completely spatially random, and hence $P[a_i | A] = \frac{1}{M}$.

When considering multiple explosions, we assumed the load is not cleared between eruptive pulses, and hence, the tephra load from each event is summed in each hazard grid cell. In this case, for K explosions, Eq. 1 can be modified to Eq. 4, while Eqs. 2 and 3 can be combined and modified to Eq. 5:

$$P[l_{E,N} > T | K \text{ eruptions from } v] \approx \sum_{j=1}^K \frac{n_j}{N_j} \tag{4}$$

$$P[l_{E,N} > T | K \text{ eruptions within } A] \approx \sum_{j=1}^K \sum_{i=1}^M \frac{n_{ij}}{N_{ij}} \times \frac{1}{M} \tag{5}$$

For Eqs. 4 and 5, the prior assumption that subsequent explosive pulses originate from a single dominant vent is used.

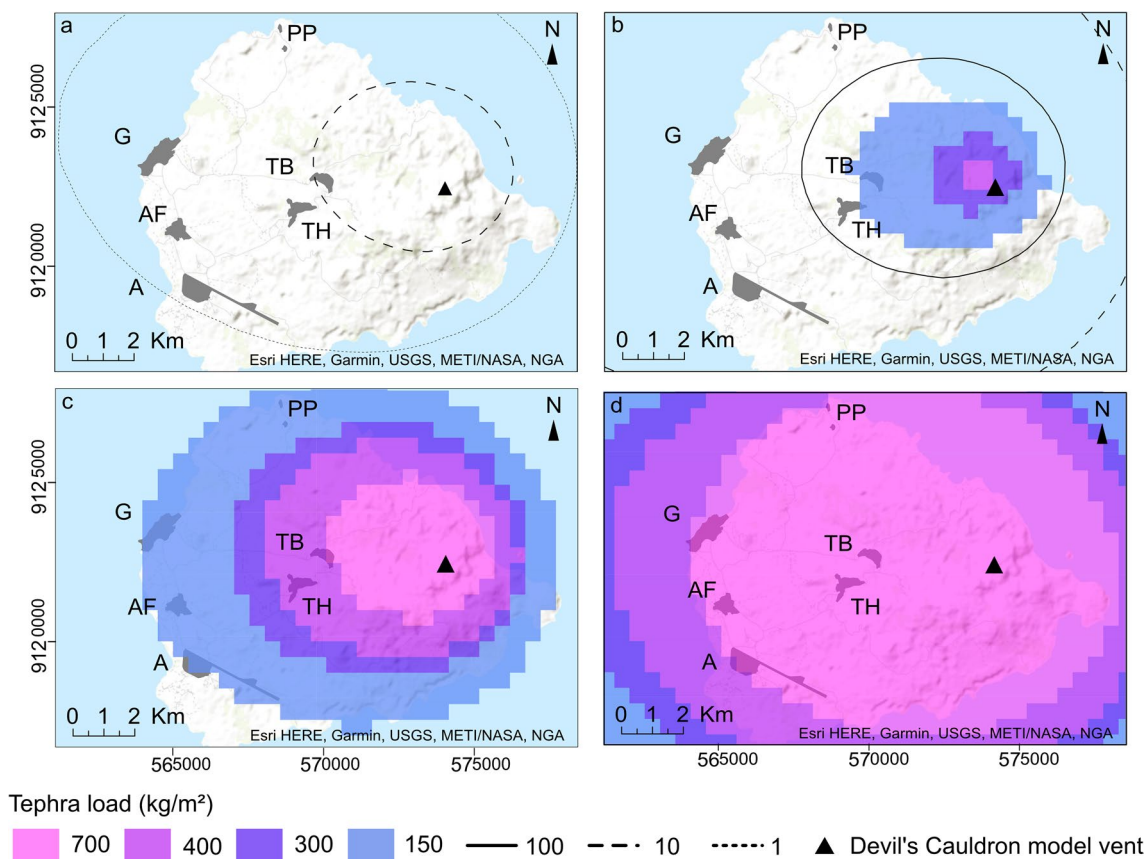
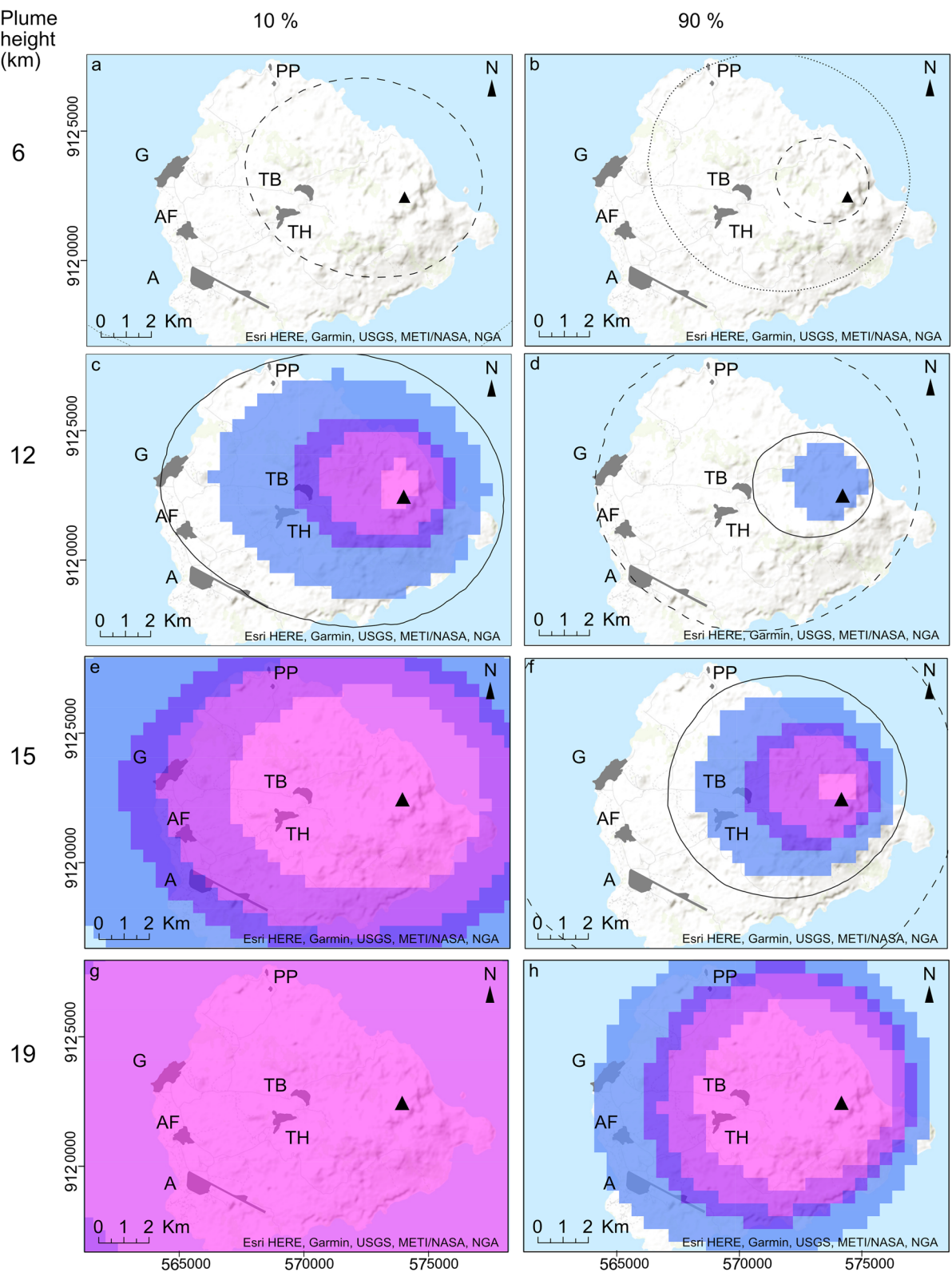


Fig. 4 Tephra ground loads with 50% probability of exceedance for trachytic event from Devil’s Cauldron with plume height **a** 6 km, **b** 12 km, **c** 15 km, **d** 19 km. Key locations: A, airport; G, Georgetown;

PP, power plant and South Atlantic Relay station; TB, Two Boats; TH, Travellers Hill; AF, US Air Force Base. Coordinate reference system: WGS84/UTM 28S

Plume height (km)



Tephra load (kg/m²)
 700 400 300 150 100 10 1 Devil's Cauldron model vent

Fig. 5 Tephra ground loads with 10 and 90% probability of exceedance respectively for trachytic event from Devil's Cauldron with plume height **a, b** 6 km; **c, d** 12 km; **e, f** 15 km; **g, h** 19 km. Key locations: A, airport; G, Georgetown; PP, power plant and South Atlantic Relay station; TB, Two Boats; TH, Travellers Hill; AF, US Air Force Base. Coordinate reference system: WGS84/UTM 28S

Output from TephraProb can be expressed as the probability of tephra mass loading exceeding a threshold or ground tephra loads given a threshold probability. Our focus is on investigating the probabilities of key reported load thresholds (Table 1) being exceeded, and therefore, we report our results as ground tephra loads with probabilities of exceedance of 10, 50 and 90%. This enables us to explore both more probable and rare-but-possible outcomes. It is important to note that the probabilistic results are explicitly linked to the modelled event(s) that we have defined. While we have selected events with a possibility of occurring on Ascension, we offer no appraisal of the likelihood of such events, or their location, simply the potential impacts of tephra loading if such an event were to occur.

Results

Felsic events

For our felsic scenarios, we present results for 6, 12, 15 and 19 km plume heights in Fig. 4 (50% probability of exceedance) and Fig. 5 (10 and 90% probability of exceedance). Results for the 27 km plume are not included in our figures, as tephra loads across the entire domain were $> 700 \text{ kg m}^{-2}$ for all probabilities. Table 4 shows ground loads at key locations and maximum proximal loads for each simulation.

Our selected model simulations from Devil's Cauldron resulted in a tephra fall covering the whole island. There was a 50% probability of loads $\geq 2 \text{ kg m}^{-2}$ for a 6 km plume height and a 90% probability of loads $\geq 1250 \text{ kg m}^{-2}$ for a plume reaching 27 km a.s.l. For our scenario with a plume height of 6 km lasting 1–3 h, there was a 50% probability of tephra loads $\geq 1 \text{ kg m}^{-2}$ over most of the island, with loads at key locations reaching threshold values ranging from 2 kg m^{-2} at Georgetown, the airport and the USAF Base to 12 kg m^{-2} at Two Boats (Fig. 4a). Loads with a 10% probability of exceedance ranged from 4 kg m^{-2} at the airport to 23 kg m^{-2} at Two Boats (Fig. 5a), and there was a 90% probability of $2\text{--}6 \text{ kg m}^{-2}$ loads at Two Boats, Travellers Hill, the power plant and South Atlantic Relay station with loads at other key locations $< 1 \text{ kg m}^{-2}$ (Fig. 5b).

For our scenario with a 12 km plume height, we found a 50% probability of tephra loads $\geq 50 \text{ kg m}^{-2}$ over the whole island with loads of 154 and 194 kg m^{-2} at Travellers Hill

and Two Boats respectively (Fig. 4b). There was a 10% probability of loads between 100 kg m^{-2} (at the airport) and 364 kg m^{-2} (at Two Boats). For a 90% probability of exceedance, loads ranged from 14 kg m^{-2} at the airport, Georgetown and the USAF Base to 93 kg m^{-2} at Two Boats (Fig. 5c, d).

Our scenario of a 1–4 h event with a 15 km plume height produced a 50% probability of tephra loads $\geq 150 \text{ kg m}^{-2}$ in all key locations, with the highest loads at Travellers Hill and Two Boats (724 and 577 kg m^{-2} respectively) (Fig. 4c). There was a 10% probability of loads $\geq 450 \text{ kg m}^{-2}$ across the whole island, with loads $> 1000 \text{ kg m}^{-2}$ at Two Boats and Travellers Hill (Fig. 5e). When considering a 90% probability of exceedance, loads ranged from 55 kg m^{-2} at Georgetown and the USAF Base to 329 kg m^{-2} at Two Boats (Fig. 5f).

For a plume height of 19 km lasting 3–6 h, we found a 50% probability of loads $\geq \sim 900 \text{ kg m}^{-2}$ and a 10% probability of loads $\geq 1800 \text{ kg m}^{-2}$ at all key locations (Figs. 4d, 5g). There was a probability of 90% of loads $\geq 1100 \text{ kg m}^{-2}$ at Two Boats and Travellers Hill, with loads of $200\text{--}350 \text{ kg m}^{-2}$ at other key locations (Fig. 5h). An event similar to Fogo A (with a plume of 27 km lasting up to 12 h) resulted in a 90% probability of loads $\geq 1250 \text{ kg m}^{-2}$ across the entire island.

Mafic events

For our mafic scenarios, figures showing a 50% probability of exceedance are presented in the main paper (Fig. 6) and figures showing a 10 and 90% probability of exceedance are included as Supplementary Material (Figs. S2–S3). Table 5 shows ground loads at key locations and maximum proximal loads for each simulation.

Single phase

For basaltic events with a plume height of 6–10 km lasting 1–6 h, our SP scenarios resulted in a 50% probability of the north and west of the island receiving a tephra load $\geq 1 \text{ kg m}^{-2}$, with values in key locations ranging from 5 kg m^{-2} at the airport to 87 kg m^{-2} at Two Boats (Fig. 6a). Loads with a 10% probability of being exceeded ranged from 18 kg m^{-2} at the airport to 231 kg m^{-2} at Two Boats, and there was a 90% probability of loads of $1\text{--}24 \text{ kg m}^{-2}$ at the key locations (Figs. S2a and S3a).

When the vent was in the AE area, we found a 50% probability of loads $\leq 1 \text{ kg m}^{-2}$ at the power plant and South Atlantic Relay station, with loads at other key locations ranging from 7 kg m^{-2} at Two Boats to 203 kg m^{-2} at the airport (Fig. 6b). For a 10% probability of exceedance, we found loads between 3 kg m^{-2} (at the power plant and South Atlantic Relay station) and 387 kg m^{-2} (at the airport) (Fig. S2b). There was a 90% probability of loads of

Table 4 Highest modelled tephra ground loads across the whole island and at key locations (maximum values within each area) for trachytic model scenarios from Devil's Cauldron (Fig. 1), with 10, 50 and 90% probability of exceedance

Plume height (km)	Probability (%)	Highest tephra ground load (kg m ⁻²)	Tephra ground load (kg m ⁻²)					
			Georgetown	Two Boats	Travellers Hill	Airport	US Air Force Base	Power plant/South Atlantic Relay station
6	10	73	5	23	17	4	5	8
	50	40	2	12	8	2	2	4
	90	21	< 1	6	4	< 1	< 1	2
12	10	790	120	364	290	100	111	143
	50	428	53	194	154	44	50	66
	90	233	14	93	69	14	14	24
15	10	2930	482	1413	1184	472	488	522
	50	1550	198	724	577	193	198	242
	90	780	55	329	241	61	55	92
19	10	9741	1952	5238	4337	1880	1943	2216
	50	6221	898	3167	2583	926	918	1067
	90	3395	221	1548	1192	308	253	350
27	90	19,024	1250	8744	6821	1890	1453	2048

82 kg m⁻² at the airport and ≤ 51 kg m⁻² across the other key locations (Fig. S3b).

For our CC single event scenario, there was a 50% probability of loads < 1 kg m⁻² at Travellers Hill, Two Boats and the airport, with Georgetown receiving 55 kg m⁻² (Fig. 6c). Loads with a 10% probability of being exceeded ranged from 6 kg m⁻² at Two Boats to 121 kg m⁻² at Georgetown (Fig. S2c). For a 90% probability, Georgetown received a load of 20 kg m⁻² and loads at the other key locations were ≤ 2 kg m⁻² (Fig. S3c).

Multiple phases

Simulations of three explosive pulses of similar plume height and duration, with no erosion or clearing of the deposit between pulses, showed a 50% probability of all key locations receiving a tephra load ≥ 20 kg m⁻² for an event from SP, with 290 kg m⁻² at Two Boats (Fig. 6d).

There was a 10% probability of all key locations except the airport receiving loads > 100 kg m⁻² and a 90% probability of loads > 100 kg m⁻² at Two Boats and Travellers Hill (Figs. S2d, S3d).

For a multi-phase event from AE, tephra loads with a 50% probability of exceedance ranged from 2 kg m⁻² at the power plant and South Atlantic Relay station to 631 kg m⁻² at the airport (Fig. 6e). There was a 10% probability of loads between 7 and 1025 kg m⁻² at key locations, with loads > 500 kg m⁻² at Travellers Hill, the airport and the

USAF Base, and a 90% probability of loads of 354 kg m⁻² at the airport, 237 kg m⁻² at the USAF Base and < 80 kg m⁻² at the other key locations (Figs. S2e and S3e).

Our multi-phase scenario from CC revealed a 50% probability of all settlements and infrastructure receiving loads ≥ 2 kg m⁻². At Georgetown, there was a 50% probability of loads reaching 176 kg m⁻² (with 10% and 90% probabilities of 278 kg m⁻² and 104 kg m⁻² loads respectively) (Figs. 6f, S2f and S3f).

Tephra loads sufficient to impact buildings

Tephra loads ≥ 100 kg m⁻² may impact buildings (Table 1), and all of our scenarios apart from the 6 km plume from Devil's Cauldron show these loads over at least part of Ascension. Table 6 and Fig. 7 show the size of the area receiving loads ≥ 100 kg m⁻² for each model scenario (with 10, 50 and 90% probabilities of exceedance). In our felsic simulations, 15–85 km² could be affected when the plume height was 12 km, while larger eruptions could result in loads ≥ 100 kg m⁻² across the whole island. For our single event mafic scenarios, there was a 50% probability that 3–11 km² could be impacted, and this increased to 28–31 km² for the three-event scenarios from SP and AE, where there was also a 10% probability of impact over 40–45 km². Three events from CC impacted 8 km² (at 50% probability) because the prevailing winds tend to disperse tephra into the sea.

Discussion

We have modelled a set of defined discrete explosive events of various plume heights from vent locations across Ascension to explore the range of tephra fall hazard footprints and impacts from such short-lived events. These events have been selected based on analogue eruptions from other small islands together with published geological data to represent a range of possible future explosive events. The results are explicitly linked to the scenarios we have chosen, and while they are within the range of possible events on Ascension, we make no assessment of the likelihood of such events, only commenting on the outputs of the models, assuming such events have occurred. A probabilistic approach to these events allows us to investigate the intrinsically variable nature of volcanic processes and atmospheric conditions which affect tephra dispersal and deposition.

Potential impact of explosive events on Ascension

Felsic events

Our results revealed that short-lived explosive events on Ascension could result in widespread tephra fall, potentially impacting the island's residents and key power, transport and communications infrastructure. Even a small felsic eruption from Devil's Cauldron, with a 6 km plume height, would impact the airport and many roads with a 50% probability of loads $\geq 1 \text{ kg m}^{-2}$ ($\sim 1 \text{ mm}$ depth, depending on deposit density) across the island (Fig. 4a and Table 1). A 12 km plume could additionally affect power and communications with our results showing a 90% probability of loads $\geq 10 \text{ kg m}^{-2}$ across the majority of the island (Fig. 5d) and a 50% probability of loads $\geq 150 \text{ kg m}^{-2}$ at Two Boats and Travellers Hill (Fig. 4b and Table 4). Previous studies have shown that, if roofs are not cleared of tephra, these loads can be sufficient to cause collapse in weak or long-span structures (Table 1 and Jenkins et al. 2014). Larger volume events could cause widespread disruption and even collapse of good quality roofs, with a 50% probability of loads $\geq 150 \text{ kg m}^{-2}$ and $\geq 700 \text{ kg m}^{-2}$ at all key locations for 15 km and 19 km plume heights respectively (Table 1 and Fig. 4c, d), necessitating extensive clean-up operations (Hayes et al. 2015).

We can compare our model results to mapped pumice fall deposits found in the east of the island. Several deposits $> 10 \text{ m}$ thick have been mapped, but only a zoned fall deposit can be correlated across the centre and east of the island, with other deposits including at Devil's Cauldron, only found in the east (Preece et al. 2021). Only our largest simulations (19 and 27 km plumes) produced maximum tephra loads $> 5000 \text{ kg m}^{-2}$ (Table 4), equivalent to deposit

thicknesses $> 10 \text{ m}$, assuming a bulk density of 500 kg m^{-3} . These simulations also produced high tephra loads across the whole island suggesting that the deposits may have been subsequently eroded, or that the eruptions occurred when winds were not from the prevailing south-easterly direction, resulting in much deposition over the sea.

Mafic events

Recent basaltic deposits came from monogenetic vents (Fig. 1) with high spatial density occurring around Sister's Peak and across the south of the island. However, limited deposit preservation makes it difficult to assess temporal relationships between vents (Vye-Brown et al. 2019). Hence, although the probability of new volcanic vents is not zero anywhere on the island, we chose to perform simulations in the three locations of most recent activity and took account of the uncertainty in the source location of a future eruption by using a grid of equally probable vent locations within those recently active areas (Fig. 2). This approach reduces the likelihood of overestimating loads proximal to the source as the results produced a smaller area where there is 90% probability of tephra fall loading sufficient to cause roof collapse ($\geq 100 \text{ kg m}^{-2}$). It also better highlights the full extent of the area that could be impacted, with a larger area having a 10% probability of tephra fall loading $\geq 100 \text{ kg m}^{-2}$.

For one basaltic event with a 6–10 km plume height, we found a 50% probability of tephra loads $> 1 \text{ kg m}^{-2}$ across the west side of the island, a deposit that could impact roads. In two of the three scenarios, the airport also received similar loads (Fig. 6a–c). There was a 10% probability of loads that may cause roof collapse ($\geq 100 \text{ kg m}^{-2}$) in the key locations closest to the vents (Fig. S2 a–c).

Our simulations investigating three phases each of 1–6 h assumed a worst-case scenario where tephra was not cleared from roofs between pulses. Areas where the impact of tephra loading is likely to depend on roof type, based on collapse loads in Table 1, are mapped in Fig. 8 (50% probability of load being exceeded) and Supplementary material Figs. S4 and S5 (10 and 90% probabilities respectively). We found a 50% probability of tephra loads in key settlements that could lead to the collapse of poor quality and long-span roofs ($\geq 150 \text{ kg m}^{-2}$) (Fig. 8a–c). We also found a 10% probability of loads that could impact good quality metal and tile roofs ($\geq 400 \text{ kg m}^{-2}$) and a 90% probability that poor quality roofs would be at risk (with loads $\geq 100 \text{ kg m}^{-2}$) (Figs. S4 and S5). In all cases, the western side of Ascension is most likely to be impacted, reflecting prevailing winds from the south-east (Fig. 8d).

We can compare our results with recent multi-phase eruptions on other small islands: St Vincent and La Palma.

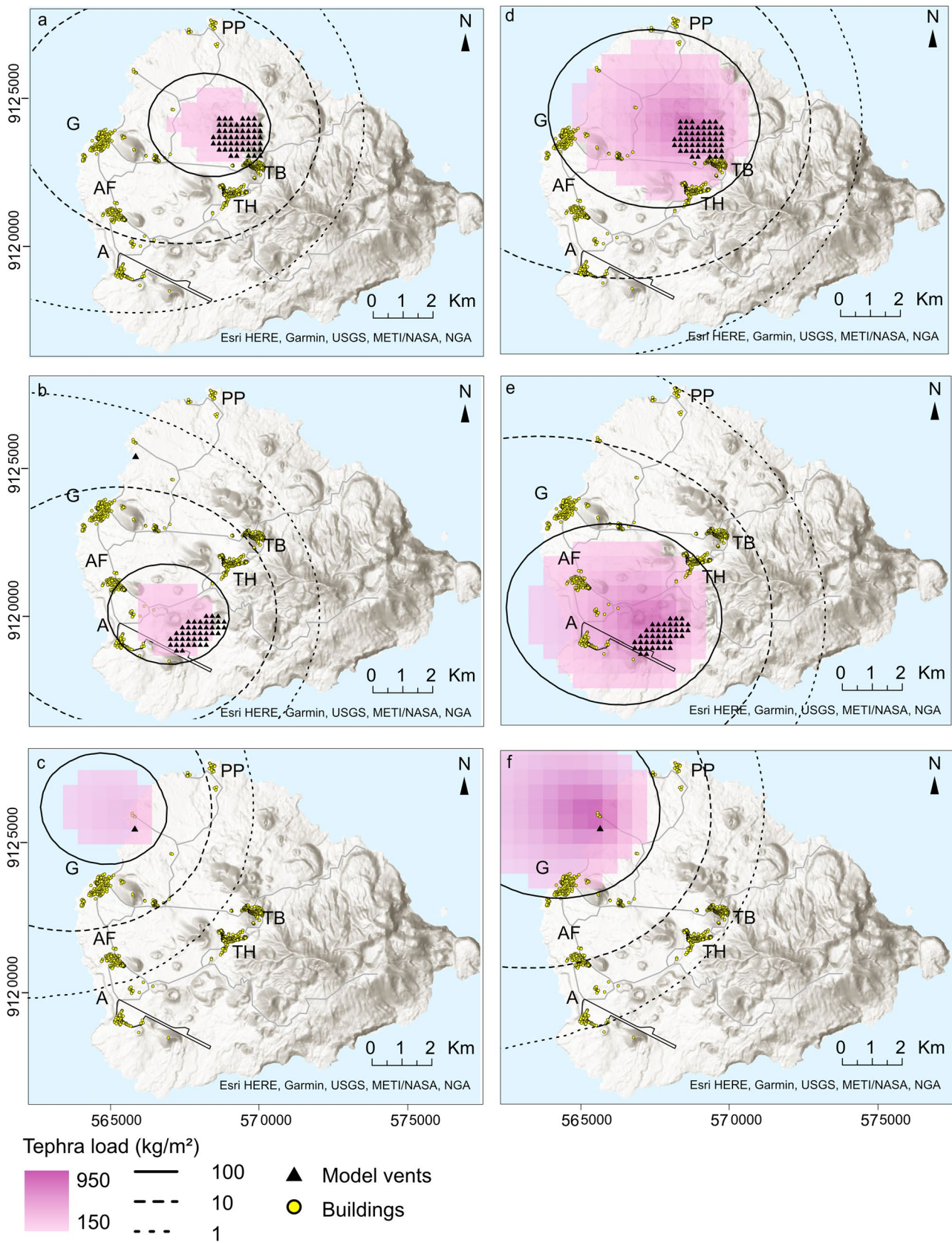


Fig. 6 Tephra ground loads with 50% probability of exceedance for basaltic events. **a, b, c** Results for one event with 6–10 km plume height; **d, e, f** results for three events, each with 6–10 km plume height, from Sister’s Peak, Airport East and Comfortless Cove respectively. For multiple events, we assume the tephra is not cleared or eroded between each pulse. Key locations: A, airport; G, Georgetown; PP, power plant and South Atlantic Relay station; TB, Two Boats; TH, Travellers Hill; AF, US Air Force Base. Coordinate reference system: WGS84/UTM 28S

The 2021 eruption of Soufrière St Vincent, with 32 discrete explosive events, highlighted how the build-up of tephra from multiple small events can create substantial proximal hazards if clean-up is not possible between eruptions (Miller et al. 2022). Fall deposits up to 70 cm thick were measured, consisting of 7 units with thicknesses of 4–27 cm (Cole et al. 2024). This equates to tephra loads of ~60–400 kg m⁻² for each unit, based on the measured deposit density of 1500 kg m⁻². Multiple pulses over a timescale of weeks were also seen during the 2021 Tajogaite eruption on La Palma with 11 tephra layers identified, each deposited over an estimated 4–13 days (Bonadonna et al. 2022; Martí et al. 2022). Layer thicknesses ≤55 cm indicate a maximum tephra load per layer of ~500–770 kg m⁻² based on the measured deposit density of 900–1400 kg m⁻². This compares to our peak loads of ~800–950 kg m⁻² for three pulses (with a 50% probability of exceedance) (Table 5).

Table 6 Area of Ascension Island (out of a total area of 98 km²) affected by tephra loads which may impact buildings (≥100 kg m⁻²) for each model scenario

Vent	Scenario	Probability of exceedance (%)		
		10	50	90
Devil’s Cauldron	6 km	0	0	0
	12 km	85	39	15
	15 km	98	96	54
	19 km	98	98	98
	27 km	98	98	98
Sister’s Peak	1 eruption	27	11	0
	3 eruptions	45	31	17
Airport East	1 eruption	25	11	0
	3 eruptions	40	28	17
Comfortless Cove	1 eruption	7	3	0
	3 eruptions	14	8	5

In this work, we have only considered the impacts of tephra fall, but within a few hundred metres of a vent, ballistics can also cause serious injury and damage to infrastructure (Fitzgerald et al. 2020; Massaro et al. 2022; Day et al. 2022). This should be investigated, given the proximity of the airport, Two Boats and Travellers Hill to the most

Table 5 Highest modelled tephra ground loads across the whole island and at key locations (maximum values within each area) (Fig. 1) for basaltic model scenarios from Sister’s Peak, Airport East and Comfortless Cove (Fig. 2) with 10, 50 and 90% probability of exceedance

Source location	No. of eruptions	Probability (%)	Highest tephra ground load (kg m ⁻²)	Tephra ground load (kg m ⁻²)					
				Georgetown	Two Boats	Travellers Hill	Airport	US Air Force Base	Power plant/South Atlantic Relay station
Sister’s Peak (SP)	1	10	445	119	231	183	18	57	114
		50	259	49	87	76	5	21	47
		90	226	15	23	24	1	6	15
	3	10	1159	298	615	473	46	143	303
		50	793	163	290	257	20	74	149
		90	495	73	107	107	7	30	73
Airport East (AE)	1	10	465	65	35	206	387	248	3
		50	282	27	7	71	203	131	<1
		90	115	9	<1	16	82	51	<1
	3	10	1191	159	89	546	1025	634	7
		50	823	92	30	240	631	412	2
		90	507	46	7	79	354	237	<1
Comfortless Cove (CC)	1	10	517	121	6	7	4	19	49
		50	313	55	<1	<1	<1	5	9
		90	147	20	<1	<1	<1	1	2
	3	10	1276	278	19	18	9	47	92
		50	953	176	2	4	3	21	47
		90	658	104	<1	<1	<1	9	18

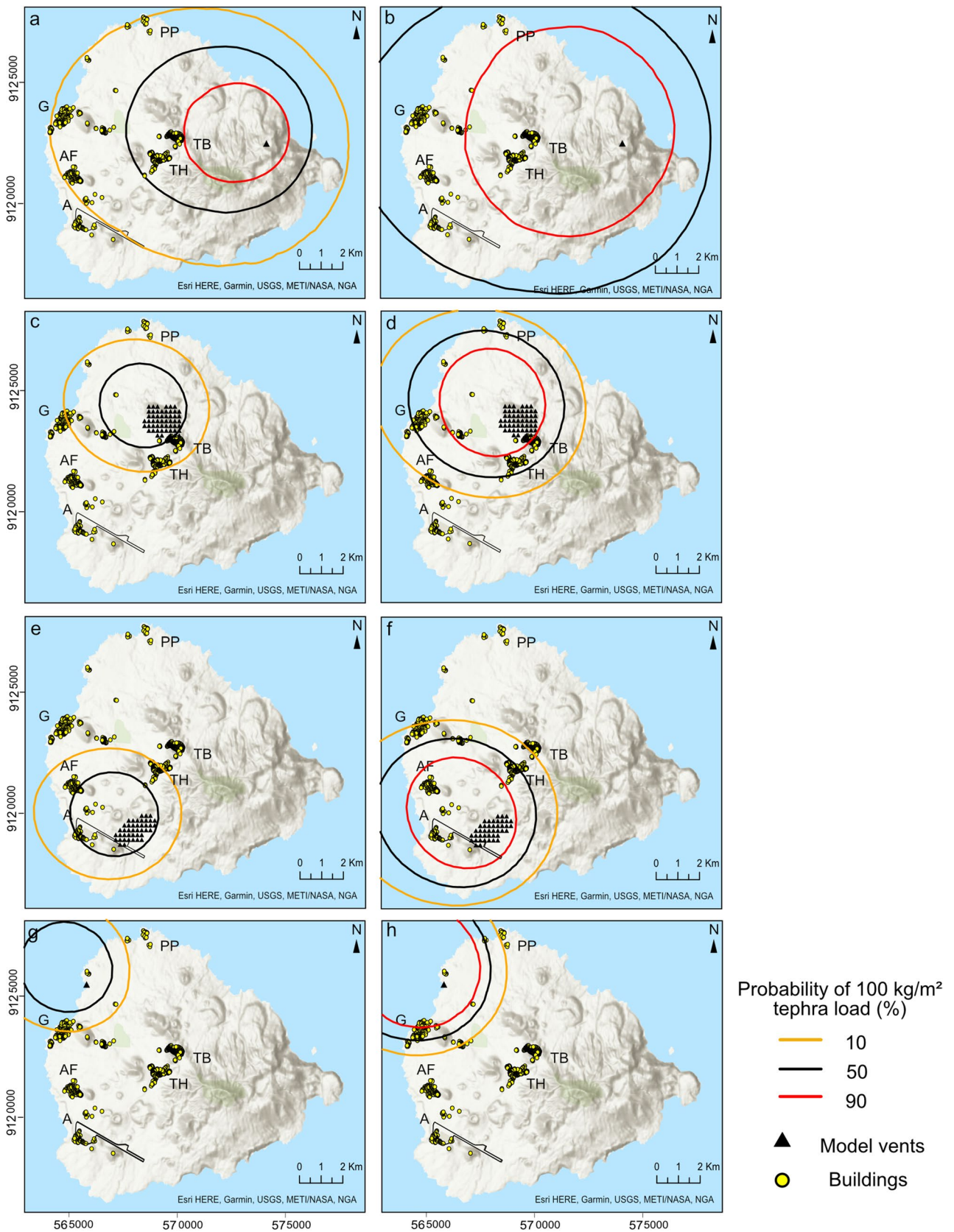


Fig. 7 Probability of tephra loads likely to impact buildings ($\geq 100 \text{ kg m}^{-2}$) for model eruption scenarios. **a, b** Results for one event from Devil’s Cauldron: (a) 12 km plume, (b) 15 km plume. **c, e, g** Results for one event with 6–10 km plume height; **d, f, h** Results for three events, each with 6–10 km plume height, from Sister’s Peak, Airport East and Comfortless Cove respectively. For multiple events, we assume the tephra is not cleared or eroded between each pulse. Key locations: A, airport; G, Georgetown; PP, power plant and South Atlantic Relay station; TB, Two Boats; TH, Travellers Hill; AF, US Air Force Base. Coordinate reference system: WGS84/UTM 28S

recent eruptive areas. Airborne ash could also lead to health issues (e.g. IVHHN 2021; Stewart et al. 2022; Eychenne et al. 2022), and the plume could have a substantial impact on airspace, particularly for larger eruptions (e.g. Witham et al. 2012; Hirtl et al. 2020; Mastin et al. 2021).

Conclusion

Small volcanic islands can be particularly susceptible to the impacts of tephra fall, given their size and potential proximity to the vent. Using Ascension as a case study, we carried out an exploratory probabilistic hazard analysis to quantify the tephra fall hazard and discuss potential impacts on infrastructure from a suite of defined eruptive events. As eruptive deposits are poorly preserved on the island, we combined existing geological data from Ascension with analogue eruptions from São Miguel, Azores, to model a wide range of possible future short-lived explosive events of both felsic and mafic composition.

Unsurprisingly, our felsic model scenarios revealed there could be significant impacts on the island, ranging from a

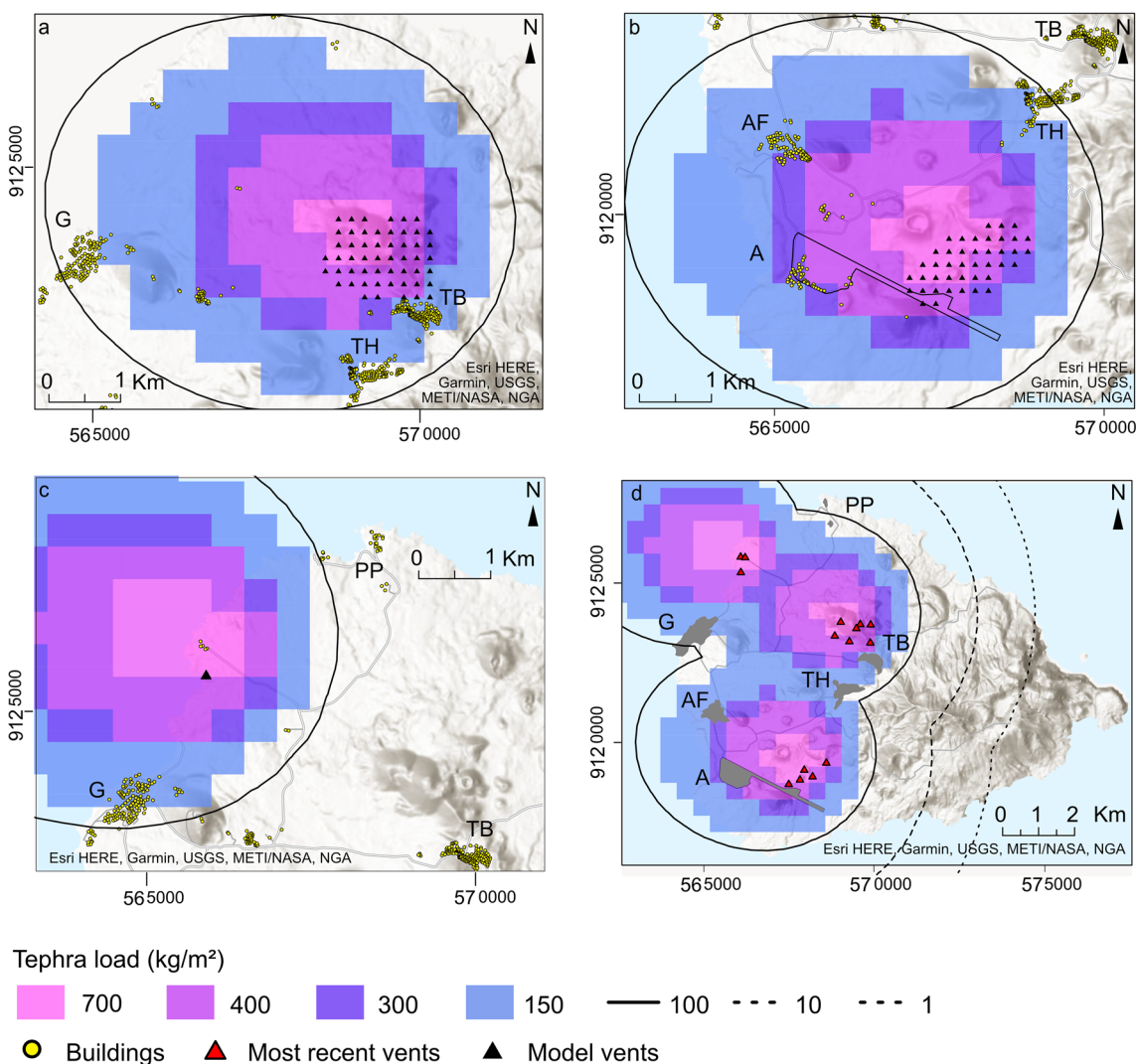


Fig. 8 Tephra ground loads likely to cause roof collapse ($\geq 150 \text{ kg m}^{-2}$) with 50% probability of exceedance for three basaltic eruptions, each with 6–10 km plume from **a** Sister’s Peak, **b** Airport East, **c** Comfortless Cove and **d** one of Sister’s Peak, Airport East and Comfortless Cove. Contours show likely collapse loads for different

roof types (Table 1). We assume the tephra is not cleared or eroded between each pulse. Key locations: A, airport; G, Georgetown; PP, power plant and South Atlantic Relay station; TB, Two Boats; TH, Travellers Hill; AF, US Air Force Base. Coordinate reference system: WGS84/UTM 28S

few millimetres of tephra fall potentially causing disruption to transport and infrastructure (for a 6 km plume), to widespread impacts including damage to key infrastructure and buildings, including potential collapse of roofs (from a 15–19 km plume).

There are numerous mafic monogenetic vents across the north, west and south of the island, but data on the temporal relationship between vents are limited. We have therefore taken account of vent uncertainty by modelling basaltic eruptions from the monogenetic volcanic field using a grid of possible vent locations within the most recently active areas. Results reveal that for an explosive event with a 6–10 km plume, there was a 50% probability that tephra fallout from a single pulse would disrupt the airport and impact roads across the west side of the island. For our scenarios comprising three distinct explosive phases, there was a 50% probability of loads that could lead to roof collapse in settlements close to the vent, assuming that roofs are not cleared between phases. In nearly all of our mafic scenarios, the airport was impacted while the eastern side of the island was least likely to be disrupted, given the prevailing wind to the west.

We have presented novel methods for quantifying tephra fall hazard on Ascension Island, using data from analogue eruptions and a grid of equally possible source locations to account for gaps in our knowledge of the island's eruptive history. We focused on loads that could lead to roof collapse and highlighted how impacts may vary with roof type. Our results are not predictive as we have no data pertaining to the likelihood of an eruption, its location, type or size, but they clearly show, given the modelling of events which may be possible on Ascension, that consideration should be given to the impact from tephra fall hazard on key infrastructure. Our approach is relevant to other low-data volcanic islands where it can assist in planning for possible future eruptions, by identifying areas most at risk from the impacts of tephra loading.

Supplementary Information The online version contains supplementary material available at <https://doi.org/10.1007/s00445-024-01771-3>.

Acknowledgements We would like to thank Charlotte Vye-Brown for discussions and her valuable insights on Ascension Island geology and infrastructure and to Katie Preece and Charles Connor for thorough and helpful reviews which enabled us to substantially improve the manuscript. This work builds on initial modelling conducted as part of a volcanic hazard analysis on Ascension Island by the British Geological Survey. JC publishes with permission of the executive director of the British Geological Survey (UKRI).

Funding SO is supported by the Leeds-York-Hull Natural Environment Research Council (NERC) Doctoral Training Partnership (DTP) Panorama under grant NE/S007458/1. This work was in part funded by the British Geological Survey University Funding Initiative (BUFI) PhD studentship S426. JC was funded by a Leverhulme Trust Research Project Grant (RPG-2013–042; PI: Jenni Barclay) and

the BGS International NC programme 'Geoscience to tackle Global Environmental Challenges', NE/X006255/1.

Data availability Relevant data are available in the tables or Supplementary information.

Code availability Not applicable.

Declarations

Conflict of interest The authors declare no competing interests.

Open Access This article is licensed under a Creative Commons Attribution 4.0 International License, which permits use, sharing, adaptation, distribution and reproduction in any medium or format, as long as you give appropriate credit to the original author(s) and the source, provide a link to the Creative Commons licence, and indicate if changes were made. The images or other third party material in this article are included in the article's Creative Commons licence, unless indicated otherwise in a credit line to the material. If material is not included in the article's Creative Commons licence and your intended use is not permitted by statutory regulation or exceeds the permitted use, you will need to obtain permission directly from the copyright holder. To view a copy of this licence, visit <http://creativecommons.org/licenses/by/4.0/>.

References

- Alatorre-Ibargüenito MA, Hernández-Urbina K, Ramos-Hernández SG (2021) Long- and short-term volcanic hazard assessment of El Chichón Volcano (Mexico) through Bayesian inference. *Nat Hazards* 106:1011–1035. <https://doi.org/10.1007/s11069-021-04506-1>
- Aravena A, Bevilacqua A, Neri A, Gabellini P, Ferrés D, Escobar D, Aiuppa A, Cioni R (2023) Scenario-based probabilistic hazard assessment for explosive events at the San Salvador volcanic complex. *El Salvador J Volcanol Geoth Res* 438:107809. <https://doi.org/10.1016/j.jvolgeores.2023.107809>
- Atkins FB, Baker PE, Bell JD, Smith DGW (1964) Oxford expedition to Ascension Island, 1964. *Nature* 204:722–724. <https://doi.org/10.1038/204722a0>
- Biass S, Bonadonna C, Connor LJ, Connor CB (2016) TephraProb: a Matlab package for probabilistic hazard assessments of tephra fallout. *J Appl Volcanol* 5:10. <https://doi.org/10.1186/s13617-016-0050-5>
- Blake DM, Deligne NI, Wilson TM, Lindsay JM, Woods R (2017) Investigating the consequences of urban volcanism using a scenario approach II: insights into transportation network damage and functionality. *J Volcanol Geoth Res* 340:92–116. <https://doi.org/10.1016/j.jvolgeores.2017.04.010>
- Bonadonna C, Connor CB, Houghton BF, Connor L, Byrne M, Laing A, Hincks TK (2005) Probabilistic modeling of tephra dispersal: hazard assessment of a multiphase rhyolitic eruption at Tarawera, New Zealand. *J Geophys Res Solid Earth* 110:B03203. <https://doi.org/10.1029/2003JB002896>
- Bonadonna C, Pistolesi M, Biass S, Voloschina M, Romero J, Coppola D, Folch A, D'Auria L, Martin-Lorenzo A, Dominguez L, Pastore C, Reyes Hardy M, Rodríguez F (2022) Physical characterization of long-lasting hybrid eruptions: the 2021 Tajogaite eruption of Cumbre Vieja (La Palma, Canary Islands). *J Geophys Res Solid Earth* 127:e2022JB025302. <https://doi.org/10.1029/2022JB025302>
- Booth B, Croasdale R, Walker GPL (1978) A quantitative study of five thousand years of volcanism on Sao Miguel, Azores. *Philos*

- Trans R Soc Lond Ser A 288:271–319. <https://doi.org/10.1098/rsta.1978.0018>
- Burgos V, Jenkins SF, Bono Troncoso L, Perales Moya CV, Bebbington M, Newhall C, Amigo A, Prada Alonso J, Taisne B (2023) Identifying analogues for data-limited volcanoes using hierarchical clustering and expert knowledge: a case study of Melimoyu (Chile). *Front Earth Sci* 11:1144386. <https://doi.org/10.3389/feart.2023.1144386>
- Carey S, Sigurdsson H (1989) The intensity of plinian eruptions. *Bull Volcanol* 51:28–40. <https://doi.org/10.1007/BF01086759>
- Cashman K, Biggs J (2014) Common processes at unique volcanoes - a volcanological conundrum. *Front Earth Sci* 2:28. <https://doi.org/10.3389/feart.2014.00028>
- Chamberlain K, Barclay J, Preece K, Brown RJ, Davidson JP (2016) Origin and evolution of silicic magmas at ocean islands: perspectives from a zoned fall deposit on Ascension Island, South Atlantic. *J Volcanol Geoth Res* 327:349–360. <https://doi.org/10.1016/j.jvolgeores.2016.08.014>
- Chamberlain K, Barclay J, Preece K, Brown RJ, Davidson JP (2019) Lower crustal heterogeneity and fractional crystallization control evolution of small-volume magma batches at ocean island volcanoes (Ascension Island, South Atlantic). *J Petrol* 60:1489–1522. <https://doi.org/10.1093/ptrology/egz037>
- Chamberlain K, Barclay J, Preece K, Brown RJ, McIntosh I, EIMF (2020) Deep and disturbed: conditions for formation and eruption of a mingled rhyolite at Ascension Island, south Atlantic. *Volcanica* 3:139–153. <https://doi.org/10.30909/vol.03.01.139153>
- Cole PD, Barclay J, Robertson REA, Mitchell S, Davies BV, Constantinescu R, Sparks RSJ, Aspinall W, Stinton A (2024) Explosive sequence of La Soufrière, St Vincent, April 2021: insights into drivers and consequences via eruptive products. Geological Society, London, Special Publications 539. <https://doi.org/10.1144/SP539-2022-292>
- Connor C, Bebbington M, Marzocchi W (2015) Probabilistic volcanic hazard assessment. In: Sigurdsson H, Houghton B, McNutt S, Rymer H (eds) *The Encyclopedia of Volcanoes*, 2nd edn. Elsevier, Oxford, pp 897–910. <https://doi.org/10.1016/B978-0-12-385938-9.00051-1>
- Connor LJ, Connor CB (2006) Inversion is the key to dispersion: understanding eruption dynamics by inverting tephra fallout. In: Mader H, Coles SG, Connor CB, Connor LJ (eds) *Statistics in Volcanology*. Geological Society, London, pp 231–242
- Constantinescu R, White JT, Connor C, Cole P, Fontijn K, Barclay J, Robertson R (2024) Estimation of eruption source parameters for the 2021 La Soufrière eruption (St Vincent): implications for quantification of eruption magnitude on volcanic islands. Geological Society, London, Special Publications 539. <https://doi.org/10.1144/SP539-2023-38>
- Crummy JM, Savov IP, Loughlin SC, Connor CB, Connor L, Navarro-Ochoa C (2019) Challenges of determining frequency and magnitudes of explosive eruptions even with an unprecedented stratigraphy. *J Appl Volcanol* 8:3. <https://doi.org/10.1186/s13617-019-0083-7>
- Daly RA (1922) The geology of Ascension and St. Helena Islands *Geol Mag* 59:146–156. <https://doi.org/10.1017/S001675680108933>
- Davies BV, Brown RJ, Barclay J, Scarrow JH, Herd RA (2021) Rapid eruptive transitions from low to high intensity explosions and effusive activity: insights from textural analysis of a small-volume trachytic eruption, Ascension Island. *South Atlantic Bull Volcanol* 83:58. <https://doi.org/10.1007/S00445-021-01480-1>
- Day JMD, Geiger H, Troll VR, Perez-Torrado FJ, Aulinas M, Gisbert G, Carracedo JC (2022) Bouncing spallation bombs during the 2021 La Palma eruption, Canary Islands, Spain. *Earth Science, Systems and Society* 2:10063. <https://doi.org/10.3389/esss.2022.10063>
- Degruyter W, Bonadonna C (2012) Improving on mass flow rate estimates of volcanic eruptions. *Geophys Res Lett* 39:L16308. <https://doi.org/10.1029/2012GL052566>
- Eychenne J, Gurioli L, Damby D, Belville C, Schiavi F, Marceau G, Szczepaniak C, Blavignac C, Laumonier M, Gardés E, Le Pennec J, Nedelec J, Blanchon L, Sapin V (2022) Spatial distribution and physicochemical properties of respirable volcanic ash from the 16–17 August 2006 Tungurahua eruption (Ecuador), and alveolar epithelium response in-vitro. *Geohealth* 6:e2022GH000680. <https://doi.org/10.1029/2022GH000680>
- Ferreira T, Gomes A, Gaspar JL, Guest J (2015) Distribution and significance of basaltic eruptive centres: São Miguel, Azores. In: Gaspar JL, Guest JE, Duncan AM, et al. (eds) *Volcanic geology of Sao Miguel Island (Azores Archipelago)*. Geological Society, London, Memoirs 44. Geological Society, London, pp 135–146. <https://doi.org/10.1144/M44.10>
- Fitzgerald RH, Kennedy BM, Gomez C, Wilson TM, Simons B, Leonard GS, Matoza RS, Jolly AD, Garaebiti E (2020) Volcanic ballistic projectile deposition from a continuously erupting volcano: Yasur Volcano, Vanuatu. *Volcanica* 3:183–204. <https://doi.org/10.30909/vol.03.02.183204>
- Gaspar JL, Guest JE, Queiroz G, Pacheco J, Pimentel A, Gomes A, Marques R, Felpeto A, Ferreira T, Wallenstein N (2015) Eruptive frequency and volcanic hazards zonation in São Miguel Island, Azores. In: Gaspar JL, Guest JE, Duncan AM, et al. (eds) *Volcanic geology of Sao Miguel Island (Azores Archipelago)*. Geological Society, London, Memoirs 44. Geological Society of London, pp 155–166. <https://doi.org/10.1144/M44.12>
- Guest JE, Gaspar JL, Cole PD, Queiroz G, Duncan AM, Wallenstein N, Ferreira T, Pacheco J-M (1999) Volcanic geology of Furnas Volcano, São Miguel, Azores. *J Volcanol Geoth Res* 92:1–29. [https://doi.org/10.1016/S0377-0273\(99\)00064-5](https://doi.org/10.1016/S0377-0273(99)00064-5)
- Harris C (1983) The petrology of lavas and associated plutonic inclusions of Ascension Island. *J Petrol* 24:424–470. <https://doi.org/10.1093/ptrology/24.4.424>
- Hayes JL, Calderón R, Deligne NI, Jenkins SF, Leonard GS, McSparran AM, Williams GT, Wilson TM (2019) Timber-framed building damage from tephra fall and lahar: 2015 Calbuco eruption, Chile. *J Volcanol Geoth Res* 374:142–159. <https://doi.org/10.1016/j.jvolgeores.2019.02.017>
- Hayes JL, Biass S, Jenkins SF, Meredith ES, Williams GT (2022) Integrating criticality concepts into road network disruption assessments for volcanic eruptions. *J Appl Volcanol* 11:8. <https://doi.org/10.1186/S13617-022-00118-X>
- Hayes JL, Wilson TM, Magill C (2015) Tephra fall clean-up in urban environments. *J Volcanol Geotherm Res* 304:359–377. <https://doi.org/10.1016/j.jvolgeores.2015.09.014>
- Hersbach H, Bell B, Berrisford P, Biavati G, Horányi A, Muñoz Sabater J, Nicolas J, Peubey C, Radu R, Rozum I, Schepers D, Simmons A, Soci C, Dee D, Thépaut J-N (2018) ERA5 hourly data on pressure levels from 1979 to present. Copernicus Climate Change Service (C3S) Climate Data Store (CDS). <https://doi.org/10.24381/cds.bd0915c6>
- Hersbach H, Bell B, Berrisford P, Hirahara S, Horányi A, Muñoz Sabater J, Nicolas J, Peubey C, Radu R, Rozum I, Schepers D, Simmons A, Soci C, Abdalla S, Abellan X, Balsamo G, Bechtold P, Biavati G, Bidlot J, Bonavita M, ... Thépaut J (2020) The ERA5 global reanalysis. *Quarterly Journal of the Royal Meteorological Society* 146:1999–2049. <https://doi.org/10.1002/qj.3803>
- Hirtl M, Arnold D, Baro R, Brenot H, Coltelli M, Eschbacher K, Hard-Stremayer H, Lipok F, Maurer C, Meinhard D, Mona L, Mulder M, Papagiannopoulos N, Pernsteiner M, Plu M, Robertson L, Roki K, Scherllin-Pirscher B, Sievers K, ... Zopp R (2020) A volcanic-hazard demonstration exercise to assess and mitigate the impacts of volcanic ash clouds on civil and military aviation. *Nat*

- Hazards Earth Syst Sci 20:1719–1739. <https://doi.org/10.5194/NHESS-20-1719-2020>
- Hobson K (2001) The pyroclastic deposits and eruption history of Ascension Island: a palaeomagnetic and volcanological study. PhD thesis, University of Oxford
- Hone DWE, Mahony SH, Sparks RSJ, Martin KT (2007) Cladistic analysis applied to the classification of volcanoes. *Bull Volcanol* 70:203–220. <https://doi.org/10.1007/s00445-007-0132-7>
- IVHHN (2021) The health hazards of volcanic ash: a guide for the public. http://ivhhn.org/images/pamphlets/Health_Guidelines_English_WEB.pdf. Accessed 2 May 2023
- Jeffery AJ, Gertisser R, O'Driscoll B, Pacheco JM, Whitley S, Pimentel A, Self S (2016) Temporal evolution of a post-caldera, mildly peralkaline magmatic system: Furnas volcano, São Miguel, Azores. *Contributions to Mineralogy and Petrology* 171:42. <https://doi.org/10.1007/s00410-016-1235-y>
- Jenkins SF, Phua M, Warren JF, Biass S, Bouvet de Maisonneuve C (2020) Reconstructing eruptions from historical accounts: Makaturing c. 1765, Philippines. *Journal of Volcanology and Geothermal Research* 404:107022. <https://doi.org/10.1016/j.jvolgeores.2020.107022>
- Jenkins SF, Spence RJS, Fonseca JFBD, Solidum RU, Wilson TM (2014) Volcanic risk assessment: quantifying physical vulnerability in the built environment. *J Volcanol Geoth Res* 276:105–120. <https://doi.org/10.1016/j.jvolgeores.2014.03.002>
- Jenkins SF, Wilson T, Magill C, Miller V, Stewart C, Blong R, Marzocchi W, Boulton M, Bonadonna C, Costa A (2015) Volcanic ash fall hazard and risk. In: Loughlin SC, Sparks RSJ, Brown SK et al (eds) *Global volcanic hazards and risk*. Cambridge University Press, Cambridge, pp 173–221
- Jicha BR, Singer BS, Valentine MJ (2013) $^{40}\text{Ar}/^{39}\text{Ar}$ geochronology of subaerial Ascension Island and a re-evaluation of the temporal progression of basaltic to rhyolitic volcanism. *J Petrol* 54:2581–2596. <https://doi.org/10.1093/ptrology/egt058>
- Kar A, Weaver B, Davidson J, Colucci M (1998) Origin of differentiated volcanic and plutonic rocks from Ascension Island, South Atlantic Ocean. *J Petrol* 39:1009–1024. <https://doi.org/10.1093/ptroly/39.5.1009>
- Kósik S, Bebbington M, Németh K (2020) Spatio-temporal hazard estimation in the central silicic part of Taupo Volcanic Zone, New Zealand, based on small to medium volume eruptions. *Bull Volcanol* 82:50. <https://doi.org/10.1007/s00445-020-01392-6>
- Kueppers U, Pimentel A, Ellis B, Forni F, Neukampf J, Pacheco J, Perugini D, Queiroz G (2019) Biased volcanic hazard assessment due to incomplete eruption records on ocean islands: an example of Sete Cidades Volcano. *Azores Frontiers in Earth Science* 7:122. <https://doi.org/10.3929/ETHZ-B-000346887>
- Ligot N, Guevara A, Delmelle P (2022) Drivers of crop impacts from tephra fallout: insights from interviews with farming communities around Tungurahua volcano, Ecuador. *Volcanica* 5:163–181. <https://doi.org/10.30909/vol.05.01.163181>
- Magill C, Wilson T, Okada T (2013) Observations of tephra fall impacts from the 2011 Shinmoedake eruption, Japan. *Earth, Planets and Space* 65:677–698. <https://doi.org/10.5047/eps.2013.05.010>
- Martí J, Becerril L, Rodríguez A (2022) How long-term hazard assessment may help to anticipate volcanic eruptions: the case of La Palma eruption 2021 (Canary Islands). *J Volcanol Geoth Res* 431:107699. <https://doi.org/10.1016/j.jvolgeores.2022.107699>
- Marzocchi W, Newhall C, Woo G (2012) The scientific management of volcanic crises. *J Volcanol Geoth Res* 247–248:181–189. <https://doi.org/10.1016/j.jvolgeores.2012.08.016>
- Massaro S, Rossi E, Sandri L, Bonadonna C, Selva J, Moretti R, Komorowski JC (2022) Assessing hazard and potential impact associated with volcanic ballistic projectiles: the example of La Soufrière de Guadeloupe volcano (Lesser Antilles). *J Volcanol Geoth Res* 423:107453. <https://doi.org/10.1016/j.jvolgeores.2021.107453>
- Mastin L, Pavolonis M, Engwell S, Clarkson R, Witham C, Brock G, Lisk I, Guffanti M, Tupper A, Schneider D, Beckett F, Casadevall T, Rennie G (2021) Progress in protecting air travel from volcanic ash clouds. *Bull Volcanol* 84:9. <https://doi.org/10.1007/S00445-021-01511-X>
- Miller VL, Joseph EP, Sapkota N, Szarzynski J (2022) Challenges and opportunities for risk management of volcanic hazards in small-island developing states. *Mt Res Dev* 42:D22–D31. <https://doi.org/10.1659/MRD-JOURNAL-D-22-00001.1>
- Minshull TA, Ishizuka O, Garcia-Castellanos D (2010) Long-term growth and subsidence of Ascension Island: constraints on the rheology of young oceanic lithosphere. *Geophys Res Lett* 37:L23306. <https://doi.org/10.1029/2010GL045112>
- Newhall C, Hoblitt R (2002) Constructing event trees for volcanic crises. *Bull Volcanol* 64:3–20. <https://doi.org/10.1007/s004450100173>
- Newhall CG, Self S (1982) The volcanic explosivity index (VEI) an estimate of explosive magnitude for historical volcanism. *J Geophys Res* 87:1231. <https://doi.org/10.1029/JC087iC02p01231>
- Nielson DL, Sibbett BS (1996) Geology of Ascension Island, South Atlantic Ocean. *Geothermics* 25:427–448. [https://doi.org/10.1016/0375-6505\(96\)00018-1](https://doi.org/10.1016/0375-6505(96)00018-1)
- Pensa A, Cas R, Giordano G, Porreca M, Wallenstein N (2015) Transition from steady to unsteady Plinian eruption column: the VEI 5, 4.6 ka Fogo A Plinian eruption, São Miguel, Azores. *J Volcanol Geoth Res* 305:1–18. <https://doi.org/10.1016/j.jvolgeores.2015.09.012>
- Preece K, Mark DF, Barclay J, Cohen BE, Chamberlain KJ, Jowitt C, Vye-Brown C, Brown RJ, Hamilton S (2018) Bridging the gap: $^{40}\text{Ar}/^{39}\text{Ar}$ dating of volcanic eruptions from the “Age of Discovery.” *Geology* 46:1035–1038. <https://doi.org/10.1130/G45415.1>
- Preece K, Barclay J, Brown RJ, Chamberlain KJ, Mark DF (2021) Explosive felsic eruptions on ocean islands: a case study from Ascension Island (South Atlantic). *J Volcanol Geoth Res* 416:107284. <https://doi.org/10.1016/j.jvolgeores.2021.107284>
- Scollo S, Tarantola S, Bonadonna C, Coltelli M, Saltelli A (2008) Sensitivity analysis and uncertainty estimation for tephra dispersal models. *J Geophys Res* 113:B06202. <https://doi.org/10.1029/2006JB004864>
- Stewart C, Damby DE, Horwell CJ, Elias T, Ilyinskaya E, Tomašek I, Longo BM, Schmidt A, Carlsen HK, Mason E, Baxter PJ, Cronin S, Witham C (2022) Volcanic air pollution and human health: recent advances and future directions. *Bull Volcanol* 84:11. <https://doi.org/10.1007/s00445-021-01513-9>
- Tadini A, Roche O, Samaniego P, Azzaoui N, Bevilacqua A, Guillin A, Gouhier M, Bernard B, Aspinall W, Hidalgo S, Eycheche J, de' Michieli Vitturi M, Neri A, Cioni R, Pistolesi M, Gaunt E, Vallejo S, Encalada M, Yepes H, ... Pique M (2021) Eruption type probability and eruption source parameters at Cotopaxi and Guagua Pichincha volcanoes (Ecuador) with uncertainty quantification. *Bull Volcanol* 83: 35. <https://doi.org/10.1007/s00445-021-01458-z>
- Tennant E, Jenkins SF, Winson A, Widiwijayanti C, Gunawan H, Haerani N, Kartadinata N, Banggur W, Triastuti H (2021) Reconstructing eruptions at a data limited volcano: a case study at Gede (West Java). *J Volcanol Geoth Res* 418:107325. <https://doi.org/10.1016/j.jvolgeores.2021.107325>

- Tierz P, Loughlin SC, Calder ES (2019) VOLCANS: an objective, structured and reproducible method for identifying sets of analogue volcanoes. *Bull Volcanol* 81:76. <https://doi.org/10.1007/s00445-019-1336-3>
- Valentine GA, Connor CB (2015) Basaltic volcanic fields. In: Sigurdsson H, Houghton B, McNutt S, Rymer H (eds) *The Encyclopedia of Volcanoes*, 2nd edn. Elsevier, Oxford, pp 423–439. <https://doi.org/10.1016/B978-0-12-385938-9.00023-7>
- Vye-Brown C, Brown R, Crummy J, Engwell S, Loughlin S (2019) Volcanic history and future hazards affecting Ascension Island. Open File Report OFR/19/026. British Geological Survey, Edinburgh
- Walker GPL, Croasdale R (1970) Two Plinian-type eruptions in the Azores. *J Geol Soc London* 127:17–55. <https://doi.org/10.1144/gsjgs.127.1.0017>
- Wardman, J, Sword-Daniels V, Stewart C, Wilson T (2012) Impact assessment of the May 2010 eruption of Pacaya volcano, Guatemala. GNS Science Report 2012/09. <https://ir.canterbury.ac.nz/handle/10092/10563>. Accessed 5 July 2023
- Warwick R, Williams-Jones G, Kelman M, Witter J (2022) A scenario-based volcanic hazard assessment for the Mount Meager Volcanic Complex. *British Columbia J Appl Volcanol* 11:5. <https://doi.org/10.1186/s13617-022-00114-1>
- Weaver B, Kar A, Davidson J, Colucci M (1996) Geochemical characteristics of volcanic rocks from Ascension Island, South Atlantic Ocean. *Geothermics* 25:449–470. [https://doi.org/10.1016/0375-6505\(96\)00014-4](https://doi.org/10.1016/0375-6505(96)00014-4)
- Widom E, Schmincke H-U, Gill JB (1992) Processes and timescales in the evolution of a chemically zoned trachyte: Fogo A, Sao Miguel, Azores. *Contrib Miner Petrol* 111:311–328. <https://doi.org/10.1007/BF00311194>
- Wild AJ, Wilson TM, Bebbington MS, Cole JW, Craig HM (2019) Probabilistic volcanic impact assessment and cost-benefit analysis on network infrastructure for secondary evacuation of farm livestock: a case study from the dairy industry, Taranaki, New Zealand. *J Volcanol Geoth Res* 387:106670. <https://doi.org/10.1016/j.jvolgeores.2019.106670>
- Williams GT, Jenkins SF, Lee DWJ, Wee SJ (2021) How rainfall influences tephra fall loading - an experimental approach. *Bull Volcanol* 83:42. <https://doi.org/10.1007/s00445-021-01465-0>
- Wilson G, Wilson TM, Deligne NI, Cole JW (2014) Volcanic hazard impacts to critical infrastructure: a review. *J Volcanol Geoth Res* 286:148–182. <https://doi.org/10.1016/j.jvolgeores.2014.08.030>
- Wilson G, Wilson TM, Deligne NI, Blake DM, Cole JW (2017) Framework for developing volcanic fragility and vulnerability functions for critical infrastructure. *J Appl Volcanol* 6:14. <https://doi.org/10.1186/s13617-017-0065-6>
- Winstanley R (2020) A preliminary investigation into the growth of the Sisters scoria cone complex, Ascension Island. M.Sc. thesis, University of Durham
- Witham C, Webster H, Hort M, Jones A, Thomson D (2012) Modelling concentrations of volcanic ash encountered by aircraft in past eruptions. *Atmos Environ* 48:219–229. <https://doi.org/10.1016/j.atmosenv.2011.06.073>